Thickness, humidity, and polarization dependent ferroelectric switching and conductivity in Mg doped lithium niobate

Sabine M. Neumayer, Evgheni Strelcov, Michele Manzo, Katia Gallo, Ivan I. Kravchenko, Andrei L. Kholkin, Sergei V. Kalinin, and Brian J. Rodriguez'

Citation: Journal of Applied Physics **118**, 244103 (2015); doi: 10.1063/1.4938386
View online: http://dx.doi.org/10.1063/1.4938386
View Table of Contents: http://aip.scitation.org/toc/jap/118/24
Published by the American Institute of Physics

Thickness, humidity, and polarization dependent ferroelectric switching and conductivity in Mg doped lithium niobate

Sabine M. Neumayer,[1,2] Evgheni Strelcov,[3] Michele Manzo,[4] Katia Gallo,[4] Ivan I. Kravchenko,[3] Andrei L. Kholkin,[5] Sergei V. Kalinin,[3] and Brian J. Rodriguez[1,2,a)]
[1]*School of Physics, University College Dublin, Belfield, Dublin 4, Ireland*
[2]*Conway Institute of Biomolecular and Biomedical Research, University College Dublin, Belfield, Dublin 4, Ireland*
[3]*Center for Nanophase Materials Sciences, Oak Ridge National Laboratory, Oak Ridge, Tennessee 37831, USA*
[4]*Department of Applied Physics, KTH Royal Institute of Technology, Roslagstullbacken 21, 10691 Stockholm, Sweden*
[5]*Department of Physics and CICECO Aveiro Institute of Materials, 3810 193 Aveiro, Portugal and Institute of Natural Sciences, Ural Federal University, 620000 Ekaterinburg, Russia*

(Received 6 October 2015; accepted 5 December 2015; published online 28 December 2015)

Mg doped lithium niobate (Mg:LN) exhibits several advantages over undoped LN such as resistance to photorefraction, lower coercive fields, and p-type conductivity that is particularly pronounced at domain walls and opens up a range of applications, e.g., in domain wall electronics. Engineering of precise domain patterns necessitates well founded knowledge of switching kinetics, which can differ significantly from that of undoped LN. In this work, the role of humidity and sample composition in polarization reversal has been investigated under application of the same voltage waveform. Control over domain sizes has been achieved by varying the sample thickness and initial polarization as well as atmospheric conditions. In addition, local introduction of proton exchanged phases allows for inhibition of domain nucleation or destabilization, which can be utilized to modify domain patterns. Polarization dependent current flow, attributed to charged domain walls and band bending, demonstrates the rectifying ability of Mg:LN in combination with suitable metal electrodes that allow for further tailoring of conductivity. © *2015 AIP Publishing LLC*.
[http://dx.doi.org/10.1063/1.4938386]

I. INTRODUCTION

Micro- and nanoscale domain engineering in lithium niobate (LN) is crucial for many applications in optics[1–4] and for the fabrication of nanostructures via photodeposition.[5–10] Due to its good nonlinear optical properties and high resistance to photorefraction,[11,12] highly Mg doped LN (Mg:LN) has gained significant interest for applications in optics as quasi phase matched devices.[13–15] Ferroelectric properties of LN change upon Mg doping and in numerous poling experiments[13,15–17] lower coercive fields and longer stabilization times for freshly poled domains[15,18,19] have been observed, as well as unidirectional high conductivity states[15,19] that were ascribed to charged domain walls.[20] However, the ferroelectric behavior that a material shows is, apart from its intrinsic properties, also strongly dependent on the presence of screening charge at polar interfaces.[21] The availability of external screening charge through ionized species from the water layer present under ambient conditions[22] has been reported to play a crucial role in ferroelectric switching.[23–29] Depending on the switching distance between applied poling pulses, periodic, intermittent, quasiperiodic or even chaotic domain patterns in LN have been observed with piezoresponse force microscopy (PFM).[28] Internal interfaces, such as those resulting from proton exchanged (PE) areas, can further lead to doping-dependent inhibition of domain growth and stability.[30–32] Introduction of periodical PE phases in undoped or doped LN is commonly applied in waveguide technology.[33–36] Tied into this structural modification is a deterioration of ferroelectricity that manifests itself as a reduced spontaneous polarization[37] that is not switchable. In this work, the impact of external screening conditions on domain sizes as well as their thickness and polarization dependence is observed using PFM to assess domain stability and band excitation (BE) first order reversal curve (FORC) spectroscopy[38–40] to track domain evolution under the application of a specifically designed waveform. Furthermore, current flow was recorded simultaneously and related to the direction of polarization.

II. MATERIALS AND METHODS

Both +z and −z 5 mol. % MgO doped congruent LN crystals of 0.5 mm thickness (Roditi Ltd.) were periodically proton exchanged along the crystallographic x-axis by exposure to benzoic acid at 230 °C for 48 h, as described elsewhere.[30,31] The maximum depth of the resulting PE channels was measured with an optical prism coupling technique to be 5.87 μm. Additionally, localized PE islands formed during the proton exchange process in the Mg:LN regions due to fine mask openings. Chemo-mechanical wedge polishing at an angle of ≈14°, using an alkaline sub-micron colloidal silica solution (SF1 Polishing Solution, Logitech), allowed cross sections of PE channels to be prepared, which preserve

a)Author to whom correspondence should be addressed. Electronic mail: brian.rodriguez@ucd.ie

the polar axis in the vertical direction and provide areas of different thickness and sample composition as schematically illustrated in Figure 1(a). A gold bottom electrode of ≈100 nm thickness was deposited through thermal evaporation in vacuum on the backside of each sample and connected via conductive silver paint to a copper circuit board.

A Veeco Dimension 3100 atomic force microscope (AFM) was used for PFM and FORC measurements. The relative humidity was adjusted to ≈12% (dry), ≈37% (ambient), and ≈65% 70% (humid) by controlling the ratio of nitrogen and water vapor in a gas cell and monitored with a humidity meter (Fluke, 971). PFM images were obtained by applying an AC voltage of 5 V at the contact resonance (≈380 kHz) generated by a function generator (Stanford Research Systems, DS345) to the tip. A lock-in amplifier (Stanford Research Systems, SR844RF) was used to demodulate the tip oscillations into PFM amplitude and phase signals with a time constant of 1 ms and a sensitivity of 3 mV. In FORC spectroscopy, a National Instruments data acquisition card (NI PXI-6115) was used to generate the combined AC and DC voltage waveform and record the electromechanical response of the cantilever at each step of the waveform. The data acquisition card was interfaced with a computer via bespoke LabVIEW and MATLAB codes. Data processing and plotting was performed in MATLAB. During FORC spectroscopy, currents were measured with a current amplifier (Femto, DLPCA-200) located between ground (GND) and the bottom electrode. Cr/Pt coated conductive tips (BudgetSensors, Mulit-75G, nominal force constant = 3 N/m, nominal resonance frequency = 75 kHz) were used

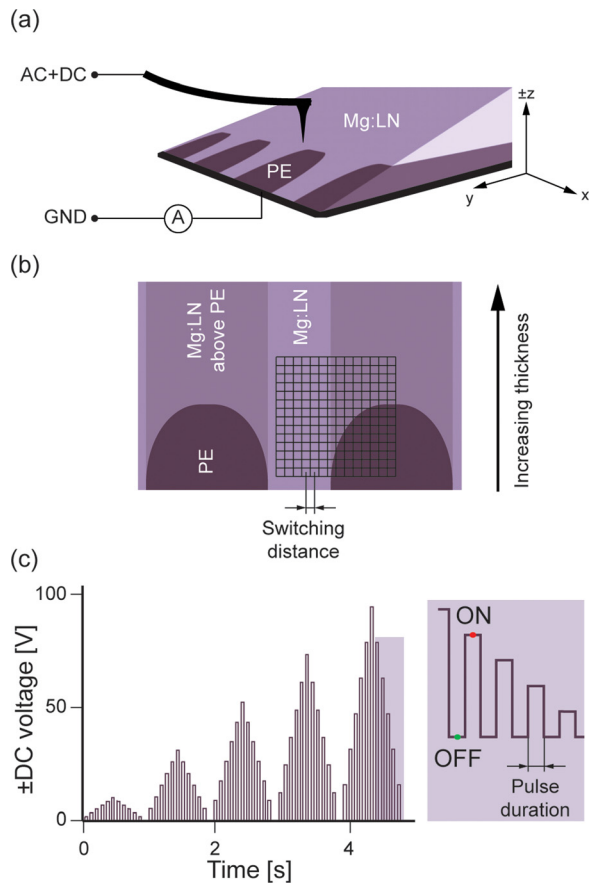

FIG. 1. (a) Schematic of the sample showing the wedge shaped Mg:LN crystal, the proton exchanged (PE) region, the AFM cantilever, and the current amplifier. (b) Schematic of the FORC grid overlaying a region of interest and defining switching distance. (c) FORC DC voltage waveform, comprising 5 triangular envelopes containing a sequence of square pulses. The zoomed in section shows the voltage ON and OFF states, during which current and PFM signals were measured, respectively.

FORC[38–40] measurements were performed on a grid of pixels overlaying a region of interest as illustrated in Figure 1(b), in order to obtain information about the domain evolution and conductivity as well as a switched domain pattern that is observable in PFM images. The voltage waveform was sequentially applied at each point of the grid. The waveform comprised 5 cycles of a unipolar triangle envelope with increasing magnitude having the same polarity as the sample consisting of square pulses of ca. 40 ms duration, as shown in Figure 1(c). The maximum pulse amplitude of 95 V available from the voltage source was chosen to test ferroelectric and conductivity behavior upon application of strong electric fields, whereas smaller envelopes of triangle square pulses with maximum values of ≈10 V, 31 V, 53 V, and 74 V allow for observations in the vicinity of the corresponding coercive field and below. Domain evolution was monitored by measuring the piezoresponse in the OFF states between DC voltage pulses. Piezoresponse signals were acquired in the BE[41] mode, and from subsequent fitting, using a simple harmonic oscillator model, PFM amplitude and phase data were extracted. The values at certain ON or OFF states for each point of the grid, where FORC pulses were applied, can then be composited into maps. Switching distances (defined in Figure 1(b)) of 1 μm, 750 nm, and 500 nm on the +z sample and 1 μm on the −z substrate were chosen. For the switching distance of 1 μm, that will be further discussed, FORC waveforms were applied in grids of $13 \times 13\ \mu m^2$ (humid condition) and $14 \times 14\ \mu m^2$ (ambient and dry conditions) over areas of different composition and thickness (Figure 1(b)).

In order to further assess correlation of phase inversion with current flow, 4 switching spectroscopy PFM (SSPFM)[42] pulses up to ±100 V in a bipolar waveform was applied to the +z sample at ambient humidity. Current flow was measured between the bottom electrode and GND while simultaneously monitoring the piezoresponse phase (at 20 kHz and 5 V).

III. RESULTS AND DISCUSSION

Consistent with prior reports,[37] the exposed PE area exhibits less piezoresponse than the surrounding Mg:LN (Figure 2). The resulting domain patterns and corresponding FORC data after application of the FORC waveform with a switching distance of 1 μm (Figure 2), yield more information than grids of higher density as domain coalescence, observed at shorter distances (Figure 3), obstructs analysis. The areas that were overlaid with the FORC grid are defined by the black indicators in the PFM amplitude images. The −z and +z crystals were studied under dry conditions (Figures 2(a) and 2(b), respectively). As the domains formed on the +z substrate did not coalesce, further experiments under ambient (Figure 2(c)) and humid conditions (Figure 2(d)) were conducted on +z. From Figure 2, several observations, discussed below, are apparent: (i)

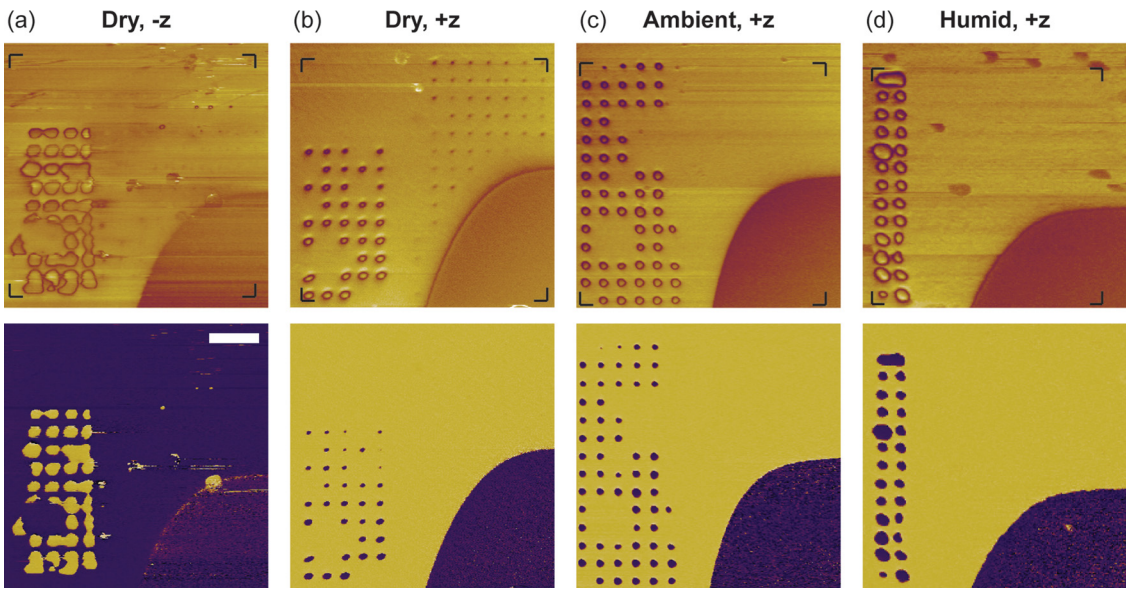

FIG. 2. PFM amplitude (first row) and phase (second row) images recorded after FORC spectroscopy on (a) the z crystal under dry conditions and the +z crystal under (b) dry, (c) ambient, and (d) humid conditions (scale bar 3 μm; amplitude color scale arbitrary; phase image color scale 180°). Black indicators in PFM amplitude images show area of FORC grids of $14 \times 14\ \mu m^2$ (dry and ambient conditions) and $13 \times 13\ \mu m^2$ (humid condition).

polarization switching is inhibited above PE layers, (ii) the domain size depends on sample thickness and humidity, and (iii) on polarization. Subsequently, current flow during ferroelectric switching is analyzed.

A. Inhibition of switching above PE

As reported previously for +z Mg:LN substrates under ambient conditions, stable ferroelectric switching is inhibited by buried PE channels and also by subsurface shallow PE islands that lead to irregular domain patterns.[32] This inhibition has been ascribed to electric fields originating from the remaining, nonswitchable polarization charge in PE that increase the energy barrier for ferroelectric switching also in the Mg:LN layer above. Polarization reversal at grid positions directly above PE is only visible as a local decrease in the PFM amplitude image on the +z sample under dry conditions. This observation suggests either domain nucleation in only a small part of the field-induced excitation volume during PFM imaging or a locally reduced upwards polarization due to misalignment of the backswitched polarization. The locations with decreased amplitude only appear at a certain distance from the exposed PE area where the Mg:LN layer above the PE interface has a thickness of >0.48 μm. A possible reason for this behavior might be lattice distortions induced by the PE phase, which have been reported to be highest in the direct vicinity of the PE channels and are also present above shallow PE islands or edges of the PE channel independent of the Mg:LN thickness.[32] These distortions could be related to strains and electromechanical coupling imposed by the PE areas.[32] While Figure 2 shows locations of stable switching, regions that may have switched and then backswitched at some stage during FORC spectroscopy are not visible. However, FORC piezoresponse maps of phase data, recorded after each DC voltage pulse, exhibit some phase inversion above the PE channel only under dry conditions at the −z and +z sample (Figures 4(a) and 4(b)), maps extracted from data after the highest pulse of ±95 V), whereas switching was not observed for +z under ambient (Figure 4(c)) or humid conditions (Figure 4(d)). From the FORC piezoresponse data, it is evident that domain switching above PE channels only occurs in a dry atmosphere when the least amount of external screening is available and the strength of the electric field is not weakened by the presence of a larger water meniscus. Above the shallow PE,

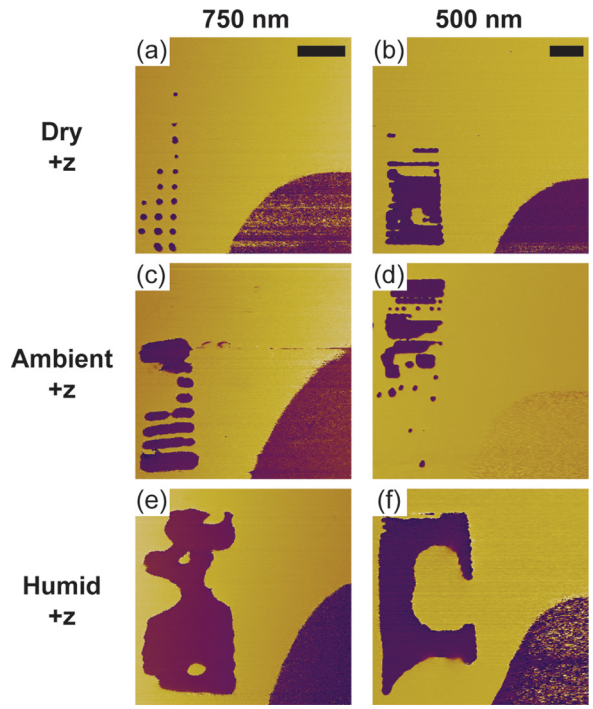

FIG. 3. PFM phase images recorded after FORC spectroscopy on the +z sample at ((a), (c), and (e)) 750 nm and ((b), (d), and (f)) 500 nm switching distances under ((a) and (b)) dry, ((c) and (d)) ambient, and ((e) and (f)) humid conditions (yellow phase contrast represents +z and purple represents z in Mg:LN; scale bars 2.5 μm).

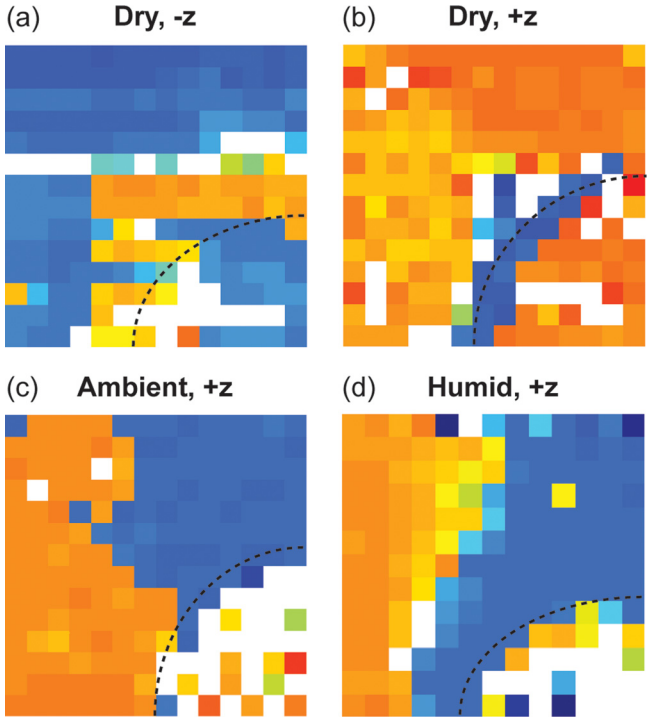

FIG. 4. BE FORC phase maps directly after the ±95 V pulse for (a) z under dry conditions and +z under (b) dry, (c) ambient, and (d) humid con ditions. Dashed line indicates the boundary of the exposed PE area. Blue corresponds to +z and orange to z. White pixels could not be fitted. The maps were acquired at areas indicated by black edges in Figure 2. Sizes are $14 \times 14\,\mu m^2$ for dry and ambient conditions ((a) (c)) and $13 \times 13\,\mu m^2$ for high relative humidity (d) (switching distance 1 μm).

phase inversion is also observed under ambient and humid conditions.

Similar to ferroelectric heterostructures,[43] the behavior of a stack of Mg:LN and PE layers between top and bottom electrodes is characterized by the internal electric fields of each layer. Polarization gradients at the internal and external interfaces lead to depolarization fields if the uncompensated bound charge is not otherwise screened.[43] Due to the absence of external screening charge in dry conditions, the depolarization field is particularly high, which is expected to lead to strong band bending and result in accumulation of holes at the PE interface and electrons at the surface. The high density of electrons at the surface, in combination with a highly localized field at the tip originating from the strongly diminished water layer, might allow for domain nucleation due to charge injection,[44,45] whereas further growth and stabilization is inhibited.

B. Domain size thickness and humidity dependence

In order to quantitatively analyze the domain size dependence on sample thickness and humidity, the surface area of each stable domain that was formed under different ambient conditions was extracted from the PFM phase images shown in Figures 2(b) 2(d) with the software *ImageJ*. Averaged size values for each row are plotted as a function of thickness for all humidities in Figure 5. Domain sizes decrease with decreasing humidity and increasing thickness as apparent from the negative slopes of linear fits in the diagram (dry:

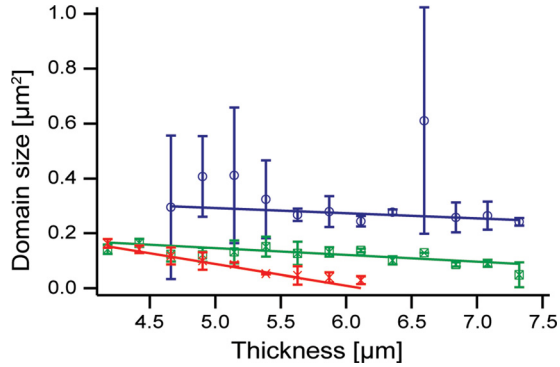

FIG. 5. Domain area as a function of sample thickness for different ambient conditions (dry: red cross, ambient: green square, humid: blue circle). Lines are linear fits of data weighted by error bars. Slopes: dry $0.783 \pm 0.082\,\mu m$; ambient $0.246 \pm 0.046\,\mu m$; humid $0.188 \pm 0.013\,\mu m$.

$-0.783 \pm 0.082\,\mu m$, ambient: $-0.246 \pm 0.046\,\mu m$, humid: $-0.188 \pm 0.013\,\mu m$). The dryer the condition, the stronger is the impact of sample thickness. The strong linear thickness dependence explains why no stable switching was observed in dry conditions above 6.1 μm, as extrapolation of the fit leads to a domain size of 0. Also, the −z sample shows switched domains only up to a thickness of ≈6.6 μm even though domain sizes are bigger and seem to be less dependent on thickness (quantitative domain size analysis is obstructed by domain coalescence).

The thickness dependence can be explained when considering that domain evolution is directed by minimization of the free energy. It comprises the domain wall energy and the interaction between tip and domain surface, and is a function of domain radius r, length l (i.e., sample thickness), and applied voltage V.[46] In order to achieve energy minimization, the ratio between length, radius, and voltage of $l/2r \sim V$ in close vicinity of the tip and $\sim V^{1/3}$ at distances exceeding the length between the center of tip curvature and sample surface must be fulfilled, as derived by Molotskii.[46] According to these relations, radii of domains in equilibrium exhibit a proportional dependence on the applied voltage and decrease with increasing sample thickness, a description that fits best the results obtained in dry conditions.

In order to understand the humidity dependence of domain sizes, the role of screening on domain evolution must be taken into account. To stabilize a nucleated domain and allow for growth, the polarization charge must be compensated by internal or external screening charge. In LN, internal screening only plays a minor role and the predominant external screening is highly dependent on adsorbates at the surface but also the availability of external screening charge from the water layer that is present on all surfaces under ambient conditions. Humidity increases the thickness of this layer and the dimensions of the water meniscus around the tip.[22,24] The water layer has been found to strongly influence ferroelectric switching as it increases the tip-sample capacitance[23] and leads to changes in the field distribution at the tip due to its conductivity[24–26] while also providing long range ionic screening charge.[27–29] From the qualitative observation that domain walls appear wider at high humidity than in dry conditions (Figure 2), a larger size of the "top

electrode" consisting of tip and water meniscus can be inferred. The apparent positive correlation between domain size and humidity has been reported previously.[23–25,29] However, also contrary observations especially at high humidity have been made,[47,48] which can be attributed to experimental conditions such as samples with higher coercive fields and switching of small sized domains that are more sensitive to the very local redistribution of the electric field caused by the water meniscus and rely less on wide range ionic screening that promotes domain growth.[48] The availability of external screening charge in ambient and humid conditions (OH on positive domain and H^+ on negative domain surfaces) stabilizes newly nucleated domains and facilitates lateral expansion.[25,48,49] This effect leads to an increase in domain sizes and apparently makes them less dependent on sample thickness.

The dependence of domain sizes on humidity also determines domain coalescence that appears at different switching distances dependent on external screening conditions. As shown in Figure 3, domains can merge independent from humidity conditions in x- and y-directions if neighboring points in the grid are only 500 nm apart (Figures 3(b), 3(d), and 3(f)). However, the 750 nm switching distance leads to three different situations: in dry conditions, no coalescence is observed (Figure 3(a)), whereas at ambient humidity (Figure 3(c)) coalescence mainly appears along the x-axis where the sample exhibits the same thickness. At high humidity, domains merge in x- and y-directions (Figure 3(e)).

Differences in domain sizes can originate from lower switching voltages (voltage at which the polarization is stably reversed) or faster domain growth. In previous SSPFM experiments in ambient conditions, an increasing switching voltage was measured for increasing sample thickness and a qualitative decrease in domain sizes was reported.[32] In order to assess whether the switching voltage is also dependent on humidity or if other effects are predominant for humidity dependence of domain sizes, the switching voltage for each stably switched domain was extracted from the FORC piezoresponse data acquired with a 1 μm switching distance under all atmospheric conditions. The average DC voltage at which stable switching occurs at a certain thickness is shown in Figure 6. On the +z sample, switching voltages appear to

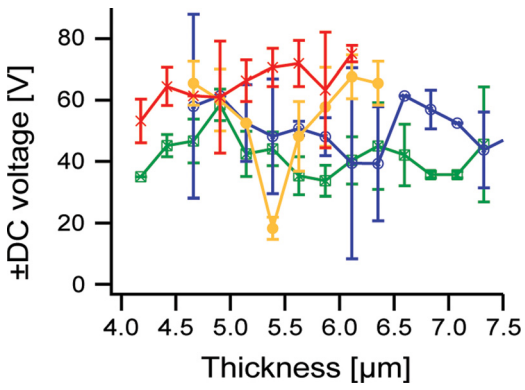

FIG. 6. ±DC voltage (+ for +z, for z Mg:LN) at which stable switching occurs as a function of sample thickness on +z (dry: red cross, ambient: green square, humid: blue circle) and z (dry: solid yellow circle) Mg:LN.

be higher in dry conditions and lower as well as more similar in ambient and humid atmospheres, but due to the strong variation of values and, in some cases, large standard deviations, a clear trend is not visible. Also, the expected thickness dependence only shows up for +z under dry conditions. The low switching voltage for −z under dry condition at a thickness of 5.39 μm might be ascribed to the presence of previously switched domains in close vicinity. From the available data, it is therefore not possible to make reliable conclusions about the exact origin of domain size differences. In principle, lower switching voltages are anticipated with increasing humidity where higher capability for external screening exists.

C. Domain size dependence of initial polarization

Domains that were switched on the −z substrate are significantly larger than on +z Mg:LN, which is consistent with prior observations of larger domain sizes for lower switching voltages and shorter pulse durations on −z compared to +z surfaces.[50] Local domain nucleation and propagation requires stabilization through screening of surface bound charge, which can be provided externally by reorientation of charge in electrodes and adsorbed ions, and also internally through bulk conductivity and charge injection.[25,28,46,51] Polarization dependent dielectric surface layers[50,52] can inhibit external screening, thus changing conditions for domain evolution.[49,51,53] However, the results suggest only a minor influence of such "dead" layers as (i) domain patterns clearly depend on external conditions such as humidity and (ii) external screening is minimized in dry conditions for which the polarization dependence was observed. Downwards band bending at a newly nucleated positive domain upon application of high negative voltages facilitates electron injection from the top electrode, which allows for screening and larger domain sizes.

D. Current flow

Apart from the insight provided by PFM, the behavior of Mg:LN as a ferroelectric semiconductor was elucidated by current measurements. High conductivity states in Mg:LN have been reported for polarization switching from up to down states[15,19] and have been ascribed to highly charged inclined head-to-head domain walls that accumulate electrons.[19,20] In the FORC experiments, high currents up to ±100 nA were measured on the +z sample at Mg:LN stripes for all atmospheric conditions (see Figures 7(b) 7(d) acquired at ±95 V). Information on the local conductivity was extracted by omitting transient currents due to polarization switching and capacitive contributions related to the square voltage pulses during FORC spectroscopy. Pixels at which currents were measured appear to also exhibit phase inversion in the FORC piezoresponse data (Figure 4), even if it is unstable. This suggests the involvement of charged domain walls as well as favorable polarization dependent band bending. The higher currents observed under humid conditions might originate from the larger electrode size and different field distribution within the thicker water layer/meniscus or concurrent Faradaic processes (e.g., water

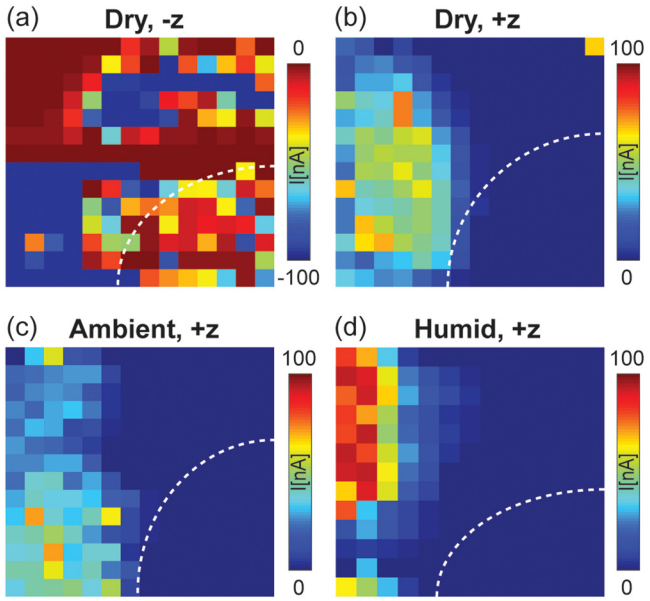

FIG. 7. FORC current maps of (a) z under dry conditions and +z under (b) dry, (c) ambient, and (d) humid conditions at ±95 V. Dashed line indicates the boundary of the exposed PE area. The maps were acquired at areas indi cated by black edges in Figure 2. Sizes are $14 \times 14\ \mu m^2$ for dry and ambient conditions (a c) and $13 \times 13\ \mu m^2$ for high relative humidity (d) (switching distance 1 μm).

splitting). Although dependence of the measured currents on the variation of the tip-sample contact and tip coating cannot be entirely ruled out, higher conductivity in humid conditions was also observed at other switching distances, indicating that the increased current can be attributed to the increased humidity. No currents were measured above the PE channels, possibly due to the low conductivity in PE areas. However, particularly high currents were observed at Mg:LN areas above shallow PE islands when the phase contrast indicated switching. Possible origins of these currents could be charged PE-Mg:LN boundaries that provide connection for the short distance to the bottom electrode or electrochemical reactions, as observed elsewhere.[54] The measured IV curves are non-Ohmic, as conductivity is often altered between the voltage cycles and ramp directions on both substrates (Figure 8). The high voltage current measurements reported elsewhere[54] showing high currents within the inner PE area and no current flow on Mg:LN do not contradict these findings. Electrochemical processes in the PE channels require activation time and voltages in the inner PE area that cannot be provided by short pulses. Furthermore, only Mg:LN regions located above the PE channel were investigated previously, where current was not detected during FORC spectroscopy either.

While current measurements on the +z sample mainly show expected behavior, the conductivity observed on the −z sample is unexpected (Figure 7(a)). Currents up to the saturation limit of the amplifier of 100 nA were measured at some areas on Mg:LN and above the PE channel. Also, no relation to polarization reversal could be made and no other data for switching from down to up state was available to verify these observations. Therefore, bipolar SSPFM pulses were applied to Mg:LN areas on the +z sample while measuring currents. Simultaneously, the SSPFM phase was acquired in order to assess if currents are polarization dependent. Figure 9(a) shows the applied voltage, corresponding PFM phase and the uncorrected currents measured during the SSPFM ON state. In this setup, currents of several nA occur at high positive voltages when the polarization is switched *down* but no currents were detected at negative voltages when the polarization is *up*, leading to a rectifying behavior. Current flow seems to start with polarization switching and the loop like behavior in IV curves (representative example of the 4th pulse shown in Figure 9(b)) might originate from the typical ferroelectric hysteresis. Furthermore, an increase in currents after the 2nd cycle is apparent, which suggests training effects on electrical and/or ferroelectric behavior.[55–57] Apart from the aforementioned conduction due to inclined head-to-head domain walls near the tip that attract electrons, band bending can also play a role. If only polarization dependent band bending is taken into account, conducting Schottky contacts are formed when positive voltages are applied to the −z domains and negative voltages to +z domains, which would lead to current flow at

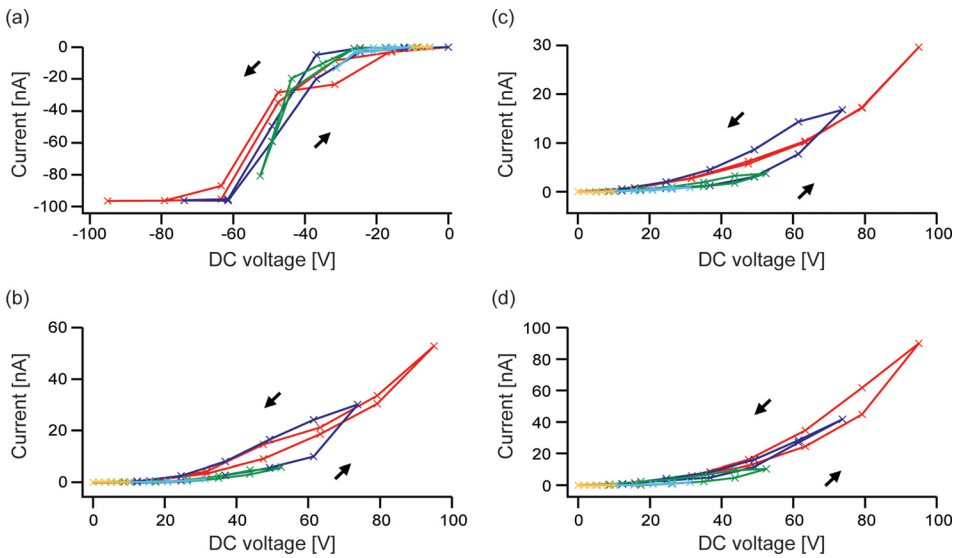

FIG. 8. Currents averaged over posi tions of stably switched domains at a thickness of ~5.87 μm: (a) z dry, (b) +z dry, (c) +z ambient, and (c) +z humid. Colors correspond to the cycle number: 1st (yellow), 2nd (light blue), 3rd (green), 4th (dark blue), and 5th (red).

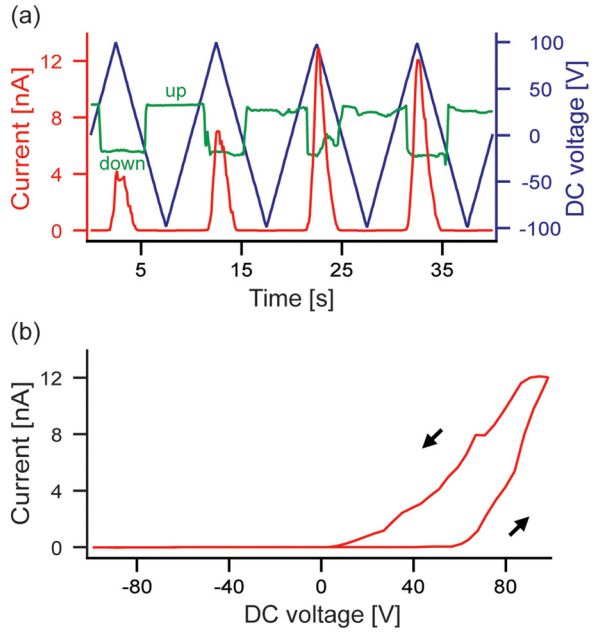

FIG. 9. Current measured in ON state of SSPFM waveform: (a) current (red), voltage (blue) and PFM phase signal acquired in OFF state (green) vs. time. (b) IV curve of 4th cycle.

all voltages that are high enough to switch independent from polarity, contrary to the results. However, if the p-type conductivity[58] of highly Mg doped LN is considered, the data are in agreement. Elsewhere, photoconductivity has been exclusively observed if the positive potential is applied to the tip.[54] These measurements were also recorded at low voltages (up to ± 10 V) under UV illumination on separate $+z$ and $-z$ samples without polarization reversal or domain walls being involved. In those experiments, the apparent downward direction of band bending at the bottom electrode independent of polarization was ascribed to p-type conductivity, whereas the tip-sample contact was considered to be Ohmic. Even if some polarization dependent band bending is taken into account, as less charge carriers are available for complete internal screening, this model can be applied to the data obtained in switching experiments: In case of a negatively poled domain, the positive surface is at the bottom electrode where downward band bending occurs due to polarization and p-type conductivity. In combination with the more negative potential at the bottom electrode, a conducting Schottky contact is established and together with the Ohmic contact at the tip side, current flow is permitted. On the other hand, if the negative domain surface is in contact with the metal (polarization *up*) and band banding still in downwards direction due to dominance of p-type conductivity, a blocking Schottky contact is formed. High currents were also measured at advanced stages of domain growth where domain walls were no longer located in direct vicinity of the tip, as indicated by PFM images and FORC piezoresponse data, which suggests that the p-type conductivity provides a major contribution to the observed conductivity. Independent of its origin, polarization dependent conductivity only appears in Mg doped, but not undoped LN and yields applications as ferroelectric Schottky diodes.[59]

IV. CONCLUSION

Switching studies on Mg:LN revealed that domain size and stability can be controlled by internal interfaces, sample thickness, atmospheric conditions, switching distance, and the initial substrate polarization. No stable domain switching was observed above the PE channel with the exception of narrow domains that appear as a reduction in amplitude on the $+z$ sample under dry conditions. A pronounced thickness dependence of domain size was apparent under dry conditions, which provides less external screening, while this effect was reduced, yet present, under ambient and humid conditions. At the same thickness, domain size increased with increasing humidity, which was mainly ascribed to a higher availability of external screening charge in a humid atmosphere. Also, domain coalescence occurred at shorter switching distances with increasing humidity. The observed domain size dependence on initial substrate polarization was attributed to charge injection from the tip into the sample at negative voltages used to switch $-z$ crystals, resulting in larger poled domains. The voltage at which stable switching occurred only showed a clear thickness dependence for the $+z$ sample in a dry environment and was accompanied by a tendency to require higher voltages required for stable polarization inversion. Currents, coupled to (temporary) polarization reversal, were measured on the $+z$ sample only in pure Mg:LN and above shallow PE islands, whereas the Mg:LN above the PE channel was not conductive. The conductivity of the tip-sample-bottom electrode system depended on the polarity of the voltage and polarization and exhibited a rectifying behavior, which was ascribed to charged inclined head-to-head domain walls that allow for high conductivity states[20] and band bending, which can be exploited in ferroelectric semiconductor devices.

ACKNOWLEDGMENTS

This research was funded by the European Commission within FP7 Marie Curie Initial Training Network "Nanomotion" (Grant Agreement No. 290158). The AFM used for this work was funded by Science Foundation Ireland (SFI07/IN1/B931). PFM and FORC measurements were conducted at the Center for Nanophase Materials Sciences, which is sponsored at Oak Ridge National Laboratory by the Scientific User Facilities Division, Office of Basic Energy Sciences, U.S. Department of Energy (user Project No. CNMS2015-139). K.G. gratefully acknowledges support from the Swedish Research Council through a Senior Fellowship (622-2010-526) and research Grant No. 621-2014-5407. A.L.K. acknowledges the CICECO-Aveiro Institute of Materials (Ref. FCT UID/CTM/50011/2013), financed by national funds through the FCT/MEC and when applicable co-financed by FEDER under the PT2020 Partnership Agreement.

[1]M. A. Arbore, M. M. Fejer, M. E. Fermann, A. Hariharan, A. Galvanauskas, and D. Harter, Opt. Lett. **22**, 13 (1997).
[2]K. R. Parameswaran, R. K. Route, J. R. Kurz, R. V. Roussev, M. M. Fejer, and M. Fujimura, Opt. Lett. **27**, 179 (2002).
[3]G. D. Miller, R. G. Batchko, W. M. Tulloch, D. R. Weise, M. M. Fejer, and R. L. Byer, Opt. Lett. **22**, 1834 (1997).

[4]K. Gallo, G. Assanto, K. R. Parameswaran, and M. M. Fejer, Appl. Phys. Lett. **79**, 314 (2001).
[5]Y. Sun and R. J. Nemanich, J. Appl. Phys. **109**, 104302 (2011).
[6]Y. Sun, B. S. Eller, and R. J. Nemanich, J. Appl. Phys. **110**, 084303 (2011).
[7]J. N. Hanson, B. J. Rodriguez, R. J. Nemanich, and A. Gruverman, Nanotechnology **17**, 4946 (2006).
[8]L. Balobaid, N. C. Carville, M. Manzo, L. Collins, K. Gallo, and B. J. Rodriguez, Appl. Phys. Lett. **103**, 182904 (2013).
[9]L. Balobaid, N. C. Carville, M. Manzo, K. Gallo, and B. J. Rodriguez, Appl. Phys. Lett. **102**, 042908 (2013).
[10]N. C. Carville, M. Manzo, S. Damm, M. Castiella, L. Collins, D. Denning, S. A. L. Weber, K. Gallo, J. H. Rice, and B. J. Rodriguez, ACS Nano **6**, 7373 (2012).
[11]D. A. Bryan, R. Gerson, and H. E. Tomaschke, Appl. Phys. Lett. **44**, 847 (1984).
[12]K. Sweeney, L. Halliburton, D. Bryan, R. Rice, R. Gerson, and H. Tomaschke, J. Appl. Phys. **57**, 1036 (1985).
[13]Y. Chen, W. Yan, J. Guo, S. Chen, G. Zhang, and Z. Xia, Appl. Phys. Lett. **87**, 212904 (2005).
[14]K. Nakamura, J. Kurz, K. Parameswaran, and M. M. Fejer, J. Appl. Phys. **91**, 4528 (2002).
[15]K. Mizuuchi, A. Morikawa, T. Sugita, and K. Yamamoto, J. Appl. Phys. **96**, 6585 (2004).
[16]M. L. Hu, L. J. Hu, and J. Y. Chang, Jpn. J. Appl. Phys., Part 1 **42**, 7414 (2003).
[17]J. H. Yao, Y. H. Chen, B. X. Yan, H. L. Deng, Y. F. Kong, S. L. Chen, J. J. Xu, and G. Y. Zhang, Phys. B Condens. Matter **352**, 294 (2004).
[18]A. Kuroda, S. Kurimura, and Y. Uesu, Appl. Phys. Lett. **69**, 1565 (1996).
[19]V. Y. Shur, I. S. Baturin, A. R. Akhmatkhanov, D. S. Chezganov, and A. A. Esin, Appl. Phys. Lett. **103**, 102905 (2013).
[20]E. A. Eliseev, A. N. Morozovska, G. S. Svechnikov, V. Gopalan, and V. Y. Shur, Phys. Rev. B: Condens. Matter **83**, 235313 (2011).
[21]M. A. Dolbilov, V. Y. Shur, E. I. Shishkin, M. F. Sarmanova, E. V. Nikolaeva, S. Tascu, P. Baldi, and M. P. de Micheli, Ferroelectrics **374**, 14 (2008).
[22]B. L. Weeks, M. W. Vaughn, and J. J. De Yoreo, Langmuir **21**, 8096 (2005).
[23]D. Dahan, M. Molotskii, G. Rosenman, and Y. Rosenwaks, Appl. Phys. Lett. **89**, 152902 (2006).
[24]A. Brugère, S. Gidon, and B. Gautier, J. Appl. Phys. **110**, 052016 (2011).
[25]V. Y. Shur, A. V. Ievlev, E. V. Nikolaeva, E. I. Shishkin, and M. M. Neradovskiy, J. Appl. Phys. **110**, 052017 (2011).
[26]B. Rodriguez, S. Jesse, A. Baddorf, S. Kim, and S. Kalinin, Phys. Rev. Lett. **98**, 247603 (2007).
[27]E. Strelcov, A. V. Ievlev, S. Jesse, I. I. Kravchenko, V. Y. Shur, and S. V. Kalinin, Adv. Mater. **26**, 958 (2014).
[28]A. V. Ievlev, S. Jesse, A. N. Morozovska, E. Strelcov, E. A. Eliseev, Y. V. Pershin, A. Kumar, V. Y. Shur, and S. V. Kalinin, Nat. Phys. **10**, 59 (2013).
[29]C. Blaser and P. Paruch, New J. Phys. **17**, 013002 (2015).
[30]M. Manzo, F. Laurell, V. Pasiskevicius, and K. Gallo, Opt. Mater. Express **1**, 365 (2011).
[31]M. Manzo, F. Laurell, V. Pasiskevicius, and K. Gallo, Appl. Phys. Lett. **98**, 122910 (2011).
[32]S. M. Neumayer, I. N. Ivanov, M. Manzo, A. L. Kholkin, K. Gallo, and B. J. Rodriguez, J. Appl. Phys. **118**, 224101 (2015).
[33]J. L. Jackel, Electron. Lett. **21**, 509 (1985).
[34]M. Digonnet, M. Fejer, and R. Byer, Opt. Lett. **10**, 235 (1985).
[35]J. L. Jackel, C. E. Rice, and J. J. Veselka, Electron. Lett. **19**, 387 (1983).
[36]S. Klauer, M. Woehlecke, and S. Kapphan, Phys. Rev. B **45**, 2786 (1992).
[37]M. Manzo, D. Denning, B. J. Rodriguez, and K. Gallo, J. Appl. Phys. **116**, 066815 (2014).
[38]I. D. Mayergoyz, Phys. Rev. Lett. **56**, 1518 (1986).
[39]O. Ovchinnikov, S. Jesse, S. Guo, K. Seal, P. Bintachitt, I. Fujii, S. Trolier Mckinstry, and S. V. Kalinin, Appl. Phys. Lett. **96**, 112906 (2010).
[40]Y. Kim, A. Kumar, O. Ovchinnikov, S. Jesse, H. Han, D. Pantel, I. Vrejoiu, W. Lee, D. Hesse, M. Alexe, and S. V. Kalinin, ACS Nano **6**, 491 (2012).
[41]S. Jesse, S. V. Kalinin, R. Proksch, A. P. Baddorf, and B. J. Rodriguez, Nanotechnology **18**, 435503 (2007).
[42]S. Jesse, A. P. Baddorf, and S. V. Kalinin, Appl. Phys. Lett. **88**, 062908 (2006).
[43]M. B. Okatan, J. V. Mantese, and S. P. Alpay, Phys. Rev. B: Condens. Matter **79**, 174113 (2009).
[44]M. Molotskii, R. Kris, and G. Rosenman, J. Appl. Phys. **88**, 5318 (2000).
[45]A. Q. Jiang, H. J. Lee, C. S. Hwang, and T. A. Tang, Phys. Rev. B: Condens. Matter **80**, 024119 (2009).
[46]M. Molotskii, J. Appl. Phys. **93**, 6234 (2003).
[47]X. Sun, Y. J. Su, K. W. Gao, L. Q. Guo, L. J. Qiao, and W. Y. Chu, J. Appl. Phys. **110**, 014103 (2011).
[48]A. V. Ievlev, A. N. Morozovska, V. Y. Shur, and S. V. Kalinin, Appl. Phys. Lett. **104**, 092908 (2014).
[49]V. Y. Shur, J. Mater. Sci. **41**, 199 (2006).
[50]D. Xue, S. Wu, Y. Zhu, K. Terabe, K. Kitamura, and J. Wang, Chem. Phys. Lett. **377**, 475 (2003).
[51]V. Y. Shur, A. R. Akhmatkhanov, I. S. Baturin, M. S. Nebogatikov, and M. A. Dolbilov, Phys. Solid State **52**, 2147 (2010).
[52]A. Y. Lushkin, V. B. Nazarenko, K. N. Pilipchak, V. F. Shnyukov, and A. G. Naumovets, J. Phys. D: Appl. Phys. **32**, 22 (1999).
[53]E. A. Eliseev, A. N. Morozovska, G. S. Svechnikov, E. L. Rumyantsev, E. I. Shishkin, V. Y. Shur, and S. V. Kalinin, Phys. Rev. B: Condens. Matter **78**, 245409 (2008).
[54]S. M. Neumayer, M. Manzo, A. L. Kholkin, K. Gallo, and B. Rodriguez, "Interface modulated currents in proton exchanged Mg doped lithium niobate" (unpublished).
[55]R. L. Gao, C. L. Fu, W. Cai, G. Chen, X. L. Deng, H. W. Yang, J. R. Sun, and B. G. Shen, Chin. Phys. B **23**, 097702 (2014).
[56]H. Zhang, W. Liu, P. Wu, X. Hai, M. Guo, X. Xi, J. Gao, X. Wang, F. Guo, X. Xu, C. Wang, G. Liu, W. Chu, and S. Wang, Nanoscale **6**, 10831 (2014).
[57]S. Goswami, D. Bhattacharya, W. Li, A. Cui, Q. Jiang, and C. Gu, Nanotechnology **24**, 135705 (2013).
[58]H. Wang, J. Wen, J. Li, H. Wang, and J. Jing, Appl. Phys. Lett. **57**, 344 (1990).
[59]P. W. M. Blom, R. M. Wolf, J. F. M. Cillessen, and M. P. C. M. Krijn, Phys. Rev. Lett. **73**, 2107 (1994).